Surfactant-assisted encapsulation of uniform SnO_2 nanoparticles in graphene layers for high-performance Li-storage

2015 2D Mater. 2 014005

(http://iopscience.iop.org/2053-1583/2/1/014005)

2D Materials

RECEIVED
15 October 2014

ACCEPTED FOR PUBLICATION
11 December 2014

PUBLISHED
13 January 2015

PAPER

Surfactant-assisted encapsulation of uniform SnO_2 nanoparticles in graphene layers for high-performance Li-storage

Wei Ai[1,2], Jianhui Zhu[1], Jian Jiang[1], Dongliang Chao[1], Yanlong Wang[1], Chin Fan Ng[1], Xiuli Wang[1], Chao Wu[1,6], Changming Li[6], Zexiang Shen[1], Wei Huang[2,4] and Ting Yu[1,3,5]

[1] Division of Physics and Applied Physics, School of Physical and Mathematical Sciences, Nanyang Technological University, 637371, Singapore
[2] Key Laboratory of Flexible Electronics (KLOFE) & Institue of Advanced Materials (IAM), National Jiangsu Synergistic Innovation Center for Advanced Materials (SICAM), Nanjing Tech University (NanjingTech), 30 South Puzhu Road, Nanjing 211816, People's Republic of China
[3] Graphene Research Centre, National University of Singapore, 117546, Singapore
[4] Key Laboratory for Organic Electronics & Information Displays (KLOEID) and Institute of Advanced Materials (IAM), Nanjing University of Posts & Telecommunications, Nanjing 210023, Jiangsu, People's Republic of China
[5] Department of Physics, Faculty of Science, National University of Singapore, 117542, Singapore
[6] Institute for Clean Energy & Advanced Materials, Southwest University, Chongqing 400715, People's Republic of China

E-mail: wei-huang@njtech.edu.cn **and** yuting@ntu.edu.sg

Keywords: SnO_2 nanoparticles, graphene, Li-ion battery, surfactant

Supplementary material for this article is available online

Abstract

SnO_2/graphene composite has been regarded as the alternative anode material for next generation high-performance lithium-ion batteries (LIBs). Here we report an efficient and facile one-pot strategy for the synthesis of SnO_2/graphene composite through a surfactant-assisted redox process. The presence of surfactant can provide homogeneous nucleation sites for SnO_2 nanoparticles formation, thus ensuring the generated SnO_2 nanoparticles have a tiny size of ~5 nm and are uniformly distributed on the graphene sheets. Simultaneously, the random aggregation of graphene sheets leads to the *in-situ* encapsulation of SnO_2 nanoparticles into graphene layers, forming a mechanically robust composite structure. These unique structural features are not only favorable for fast electrons transport and Li ions diffusion, but also capable of effectively buffering the volume changes of SnO_2 nanoparticles. As a consequence, the SnO_2/graphene composite exhibits superior Li storage performance in terms of large reversible capacity, good cycling stability and excellent rate capability.

1. Introduction

Since their birth in the early 1990s, lithium-ion batteries (LIBs) have been extensively used as the primary power source for portable electronics ranging from digital cameras and mobile phones to laptop computers, due to their significant advantages over other traditional batteries [1]. Despite these notable successes, a sustainable world still requires lighter, smaller, cheaper and more efficient LIBs with more power that can compete with traditional fossil fuels for powering electric vehicles. However, the current electrochemical performance (e.g. limited Li storage capacity, poor rate capability, etc) of commercially utilized graphite anode is insufficient to meet these requirements [2]. To this end, intense efforts have been focused on the research and development of alternative anode materials for next generation LIBs. SnO_2 is regarded as one of the most promising candidates due to its high Li storage capacity (782 mAh g^{-1}), low discharge potential, non-toxicity and low cost [3]. Unfortunately, the practical application of SnO_2 anode suffers from a severe pulverization-induced capacity fading, arising from its large volume changes (~300%) and agglomeration during the repeated Li insertion/extraction process [4]. To address these issues, researchers have proposed several approaches to improve the electrochemical performance of SnO_2. Owing to the high surface area to volume ratio, nanostructured materials offer

significance advantages over their bulk counterparts, since smaller particles can decrease the deformation of the electrode material and endow better electrochemical performance [5]. In this regard, the morphologically engineering of SnO_2 into various nanostructures have been performed to achieve improved performances including nanocubes [6], nanotubes [7], nanowires [8], porous [9] and hollow nanoparticles [10]. Nevertheless, the complicated fabrication procedures and relatively high costs hinder the large-scale production and commercialization of these nanostructures.

Another effective strategy is to fabricate SnO_2-based composites by coating other stable metal oxides [11, 12] or conductive carbon-based matrices [13, 14]. In particular, the introduction of carbon-based materials (e.g. carbon nanofiber, mesoporous carbon, carbon nanotube and graphene) can not only improve the conductivity of SnO_2 nanoparticles but also prevent their agglomeration, as well as buffer the associated volume changes [15, 16]. Among these carbon-based materials, graphene has received enormous attention due to its special two-dimensional geometric structure and fascinating physical and chemical properties [17, 18]. So far, various techniques have been developed to fabricate SnO_2/graphene composites, such as the hydrothermal method [19, 20], physical mixing method [21], solution-based synthesis method [22, 23] and ball-milling method [24]. However, the electrochemical performance of SnO_2/graphene composites is still not satisfying due to: (i) the SnO_2 nanoparticles are only simply decorated on the surface of graphene in most cases rather than confined in graphene layers, making them easily peeled off from the graphene sheets during long-term cycling [25, 26]. (ii) The inhomogeneous size distribution of SnO_2 nanoparticles makes it difficult for the graphene sheets to effectively prevent their agglomeration within electrodes because of the high surface energy [27]. Until now, SnO_2/graphene composites with uniform structure and thus superior electrochemical performance, especially high rate capability have rarely been achieved [28].

In this work, we develop a facile one-pot approach for the synthesis of SnO_2/graphene composite via a surfactant-assisted redox process. The SnO_2 nanoparticles are formed via Sn^{2+}-induced reduction of graphene oxide (GO), and simultaneously encapsulated into graphene layers due to the random aggregation of graphene sheets. Furthermore, the presence of surfactant is indispensable for guaranteeing the uniformity of SnO_2 nanoparticles with a tiny size of ~5 nm and homogeneous distribution on graphene sheets. As expected, the resultant SnO_2/graphene composite exhibits superior Li storage properties with large reversible capacity, good cyclic lifespan and excellent rate capability, highlighting its great potential applications in future LIBs.

2. Experimental section

2.1. Preparation of GO

GO was obtained via the oxidation of natural graphite (China Jixi Jinyu Graphite Co., Ltd) using a modified Hummers' method, and purified by dialysis for one week [29].

2.2. Preparation of surfactant-assisted encapsulation of SnO_2 nanoparticles in graphene layers (SAE SnO_2/G)

1 g hexadecyltrimethylammonium bromide (HTMAB) was dispersed in 150 mL GO aqueous solution (~0.5 mg mL^{-1}) under stirring at 40 °C. Subsequently, 14 mL ethanol solution of $SnCl_2$ (500, 250 and 125 mg) was dropwised into the solution, and then further stirred at 40 °C for 2 h. Finally, the obtained products were collected by centrifugation and repeat washing with deionized water several times, and dried in an oven at 100 °C for 12 h. The resultant powders were denoted as SAE SnO_2/G-6.7, SAE SnO_2/G-3.3 and SAE SnO_2/G-1.7, respectively, according to the mass ratio of $SnCl_2$ and GO.

2.3. Preparation of SnO_2 nanoparticles decorated graphene (SnO_2/G)

For comparison, SnO_2/G was prepared under the same condition as SAE SnO_2/G (3.3) except for the absence of HTMAB, and denoted as SnO_2/G-3.3.

2.4. Characterization

Field-emission scanning electron microscopy (FESEM) images were obtained using a JEOL JSM-6700 F electron microscope. Transmission electron microscopy (TEM) observations were carried out on a JEOL JEM-2010 high resolution transmission electron microscope (operated at 200 kV). X-ray photoelectron spectroscopy (XPS) analysis was conducted on a Perkin-Elmer model PHI 5600 XPS system using an Al Kα (1486.6 eV) x-ray source. The crystal phase of the products was characterized by powder x-ray diffraction (XRD) with Cu Kα radiation ($\lambda = 1.54184$ Å). Thermogravimetric analysis (TGA) was carried out on a Shimadzu DTG-60 H instrument at a heating rate of 10 °C min^{-1} in air. Raman spectra were recorded on a WITEC CRM200 Raman system with 457 nm excitation laser.

2.5. Electrochemical characterizations

Electrochemical tests were measured using coin-type cells (CR 2032) assembled in an argon-filled glove box with Li foil as the counter and reference electrode, 1 M $LiPF_6$ in a 50:50 (w/w) mixture of ethylene carbonate and dimethyl carbonate as the electrolyte. The working electrodes were prepared by a slurry coating procedure. Typically, active material, acetylene black and polyvinylidene fluoride, were mixed at a weight ratio of 80:10:10 in N-methyl-2-pyrrolidinone solvent to

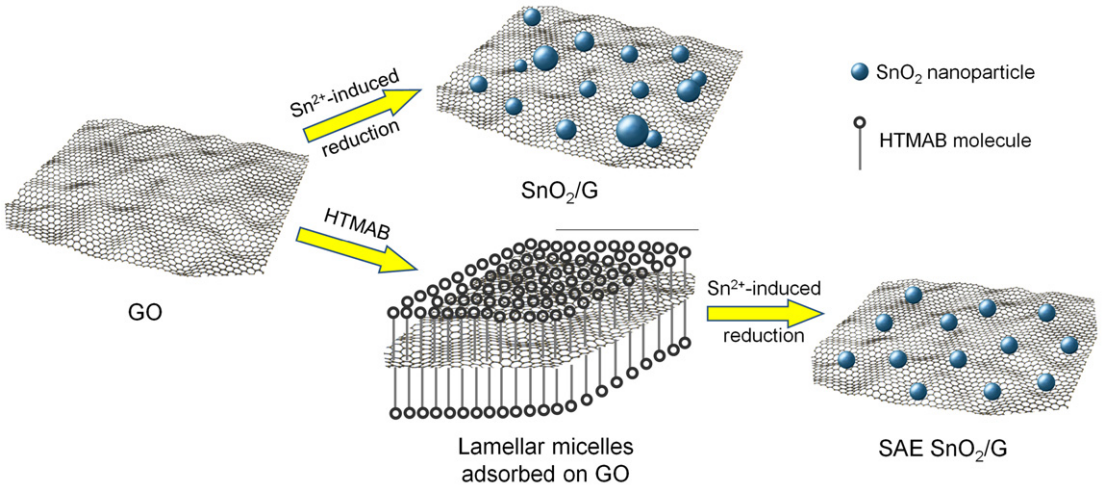

Scheme 1. Schematic illustration of the fabrication of SnO_2/G and SAE SnO_2/G composites.

form slurry. The slurry was then uniformly spread onto a copper foil current collector and dried in a vacuum oven at 100 °C for 12 h. Circular electrodes with a diameter of 1.2 cm were punched out using an electrode punch. The mass of the active material on each electrode was 1.2–1.5 mg. Galvanostatic charge-discharge tests were carried out on a NEWARE battery testing system. Cyclic voltammogram (CV) and electrochemical impedance spectroscopy (EIS) measurements were performed on CHI 760D electrochemical workstation.

3. Results and discussion

The fabrication of SnO_2/G and SAE SnO_2/G composites is schematically illustrated in scheme 1. Briefly, the composites were prepared via redox reaction between GO and Sn^{2+}, which results in the reduction of GO into graphene and the oxidation of Sn^{2+} to SnO_2. Normally, the preparation of SnO_2/G composite by Sn^{2+}-induced reduction is conducted by mixing GO dispersion with the Sn^{2+} ions [30]. Due to the electrostatic forces, Sn^{2+} ions are captured by the oxygen-containing functional groups on GO, and then the redox reaction occurs. However, the randomly distributed oxygen-containing functional groups leads to the generation of multiple nucleation sites and thus inhomogeneous distribution of SnO_2 nanoparticles, yielding unsatisfied electrochemical performance of SnO_2/G [31]. The improved method we proposed here is to introduce a cationic surfactant HTMAB. In this process, the positively charged hexadecyltrimethylammonium ions of HTMAB would be firstly absorbed on the basal plane of GO, forming lamellar micelles with a sandwich-like structure. The close-packed micelles not only serve as homogeneous nucleation sites for SnO_2 nanoparticles formation, but also prevent their further growth or agglomeration, resulting in a uniform distribution of SnO_2 nanoparticles loaded on graphene sheets. In addition, the random aggregation of graphene sheets ensures the formation of SAE SnO_2/G and hence excellent Li-storage properties. In addition, this method is more efficient and effective than conventional solution-based synthesis method [22, 23], as high-temperature annealing treatment for phase-purity/crystallinity is not required.

The morphologies of the as-prepared SnO_2/G and SAE SnO_2/G samples were investigated by FESEM and TEM. Figures 1(a), 2(a) and (b) reveal that the SnO_2/G-3.3 composite presents a large number of SnO_2 nanoparticles on graphene layers with the size varying from several nanometers to dozens of nanometers. As discussed above, the wide particle-size distribution range is mainly due to the multiple nucleation sites for SnO_2 nanoparticles formation. After the introduction of surfactant, the aggregation of SnO_2 nanoparticles does not appear in the SAE SnO_2/G-1.7 and SAE SnO_2/G-3.3 composites (figures 1(b) and (c)), thus only randomly aggregated graphene sheets are observed. However, a large excess of Sn^{2+} precursor in the composite (SAE SnO_2/G-6.7) will induce further growth or agglomeration of SnO_2 nanoparticles (figure 1(d)). TEM and HRTEM images (figures 2(c) and (d)) disclose the homogenous distribution of SnO_2 nanoparticles on the graphene layers with a uniform size of ~5 nm in the SAE SnO_2/G-3.3 composite, demonstrating the importance of the introduced surfactant for the formation of SnO_2 nanoparticles.

The SnO_2/G and SAE SnO_2/G composites were further analyzed by XPS, XRD and Raman spectroscopy to investigate their structural characteristics. From the XPS survey spectra (figure 3(a)), C, O and Sn are clearly detected in the composites. Meanwhile, the Sn 3d spectra of the composites (figure 3(b)) show two symmetric peaks at about 487.6 and 496.0 eV, corresponding to the Sn 3d5/2 and Sn 3d3/2 peaks, respectively [32]. The energy splitting between the two peaks

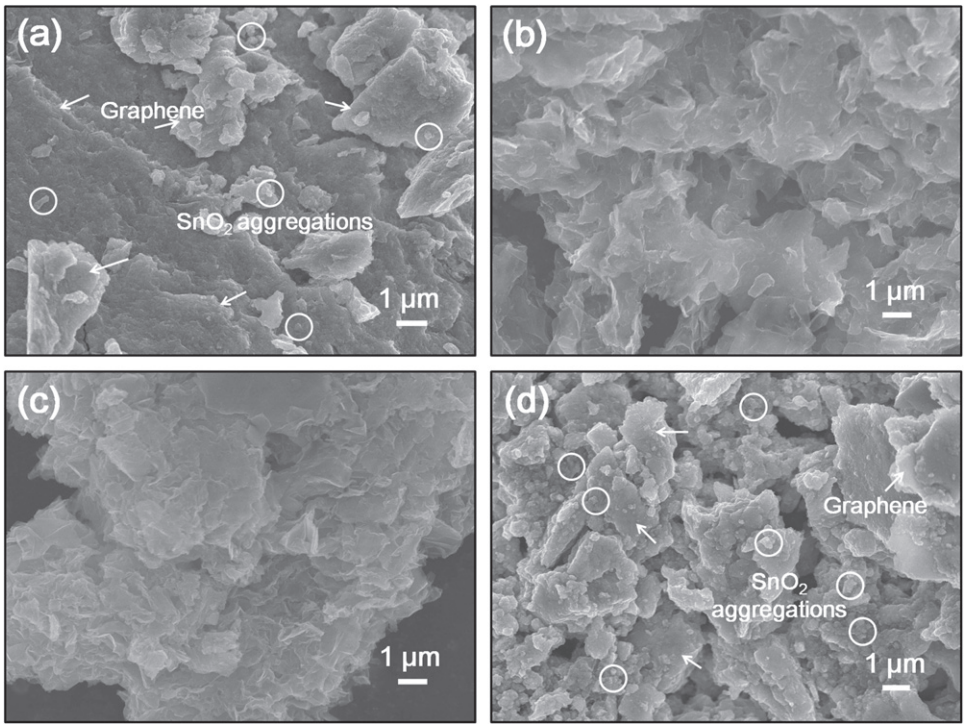

Figure 1. SEM images of SnO_2/G-3.3 (a), SAE SnO_2/G-1.7 (b), SAE SnO_2/G-3.3 (c) and SAE SnO_2/G-6.7 (d) composites.

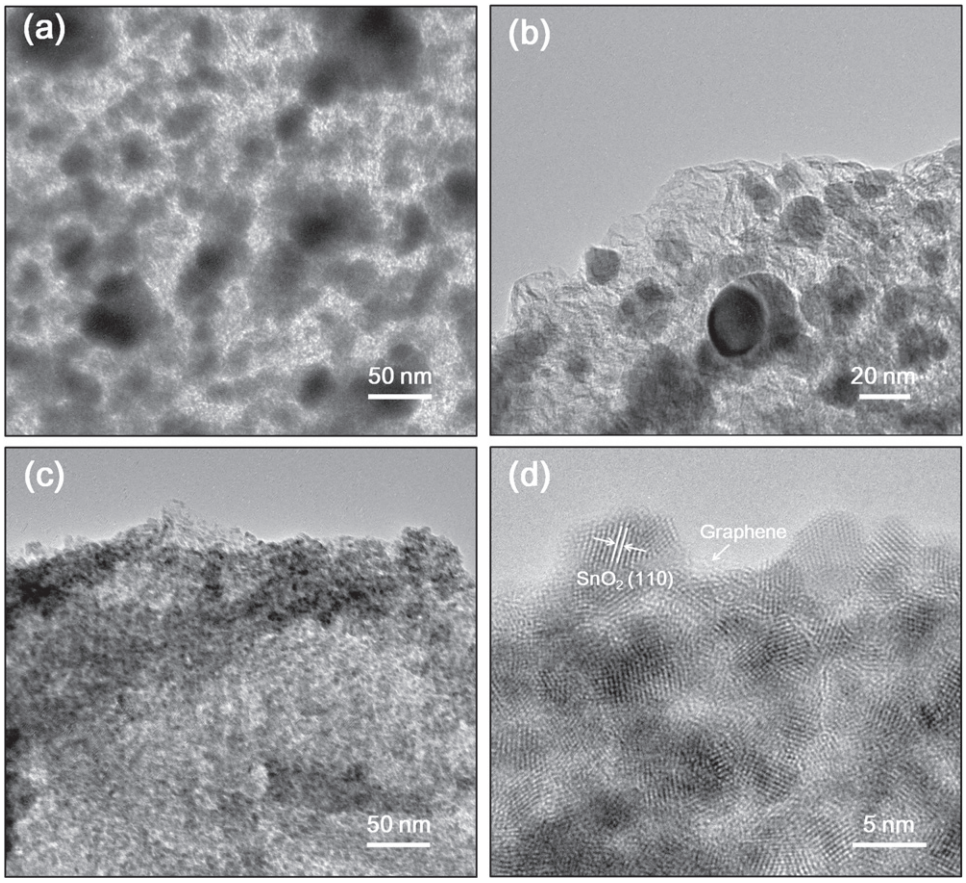

Figure 2. TEM images of SnO_2/G-3.3 composite (a) and (b). TEM image (c) and HRTEM image (d) of SAE SnO_2/G-3.3 composite.

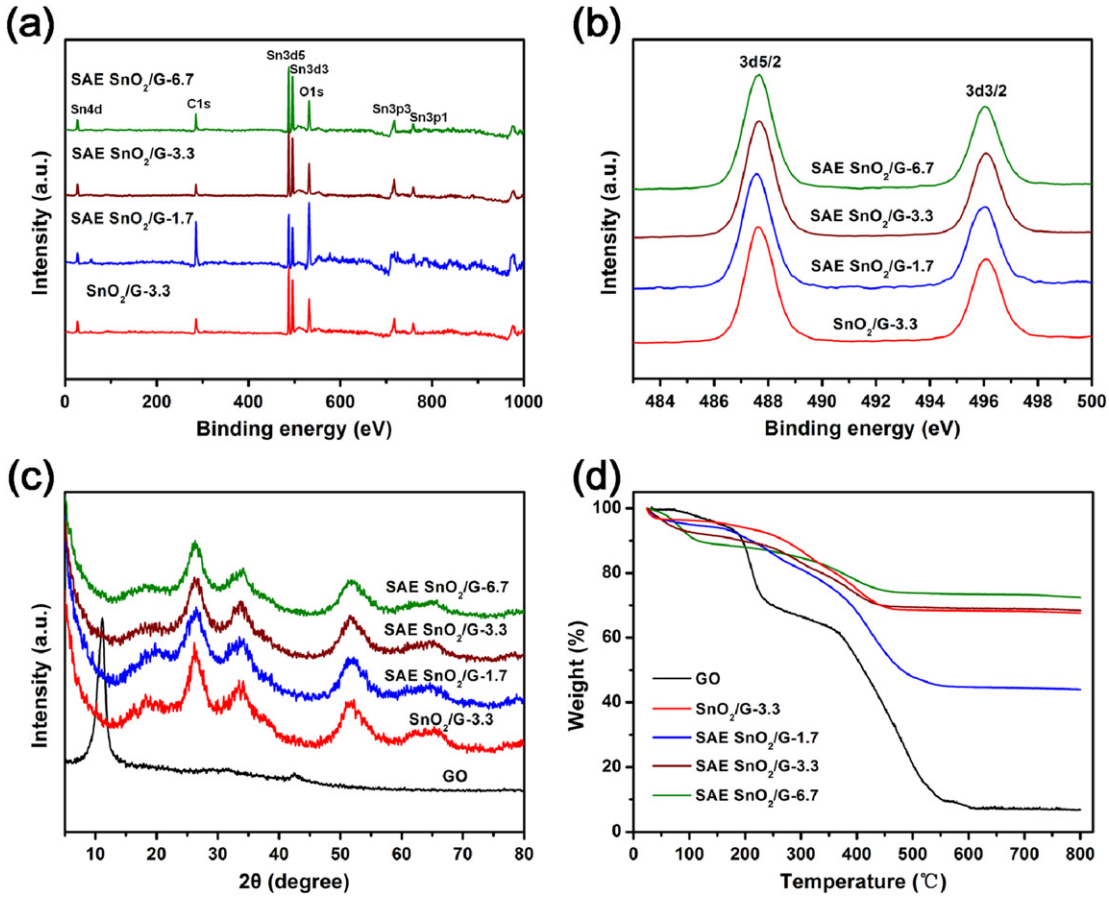

Figure 3. (a) XPS survey spectra of SnO_2/G and SAE SnO_2/G composites. (b) XPS Sn 3d spectra of SnO_2/G and SAE SnO_2/G composites. (c) XRD patterns of GO, SnO_2/G and SAE SnO_2/G composites. (d) TGA curves of GO, SnO_2/G and SAE SnO_2/G composites.

is 8.4 eV, indicating the formation of SnO_2 nanoparticles [30, 33]. Figure 3(c) shows the XRD patterns of samples. GO exhibits a characteristic diffraction peak at $2\theta = 11°$ due to the intercalation of oxygen-containing functional groups between graphene sheets. The diffraction peaks of the composites at $2\theta = 26.3°$, 33.4°, 51.9° and 65.5° can be successively assigned to the (110), (101), (211) and (301) planes of the SnO_2 phase (JCPDS No. 41–1445) [34], further confirming the formation of SnO_2 nanoparticles. The significant structural changes of GO after the redox process were detected by Raman spectroscopy. As shown in figure S1 (available in the supplementary data), the Raman spectrum of GO contains both a D band at 1356 cm^{-1} (k-point phonons of A_{1g} symmetry) and a G band at 1584 cm^{-1} (E_{2g} phonon of sp^2 atoms), with a I_D/I_G ratio of 0.84 [2, 18]. Notably, the frequencies of the D and G bands in the composites do not show any relative shifts in comparison with that observed in GO. However, an increased I_D/I_G ratio is observed in the composites, which is attributed to the formation of numerous small sp^2 domains in graphene sheets after Sn^{2+} induced reduction [35, 36].

To determine the content of graphene in the composites, TGA was carried out in air. As shown in the TGA curves (figure 3(d)), the initial mass loss of the samples below 100 °C is due to the loss of adsorbed water. A rapid mass loss can be observed with the increase of the temperature from 100 to 700 °C, which is assigned to the combustion of graphene in air (yielding CO_2) [19, 37]. The content of graphene in these composites is calculated to be 28%, 51%, 24% and 18% for SnO_2/G-3.3, SAE SnO_2/G-1.7, SAE SnO_2/G-3.3 and SAE SnO_2/G-6.7, respectively.

Electrochemical Li storage properties of the composites were evaluated by using CR2032 type coin cells. Figure 4 shows the first three CV curves for the SnO_2/G and SAE SnO_2/G electrodes at a scan rate of 0.5 mV s^{-1}. The cathodic peak at ~0.9 V in the first cycle is due to the formation of solid electrolyte interphase (SEI) and reduction of SnO_2 to Sn [20]. This peak disappeared in the following cycles, and a new reversible peak at ~1 V is observed, indicating the conversion reaction of SnO_2 [28]. While the peak at ~0.02 V can be ascribed to the alloying reaction of Sn with Li to form various Li_xSn alloys [38]. In the anodic sweep, two peaks at ~0.6 and ~1.3 V are observed. The first peak corresponds to the dealloying reaction of Li_xSn alloys, whereas the second peak represents the partially reversible reaction of SnO_2 with Li [39, 40].

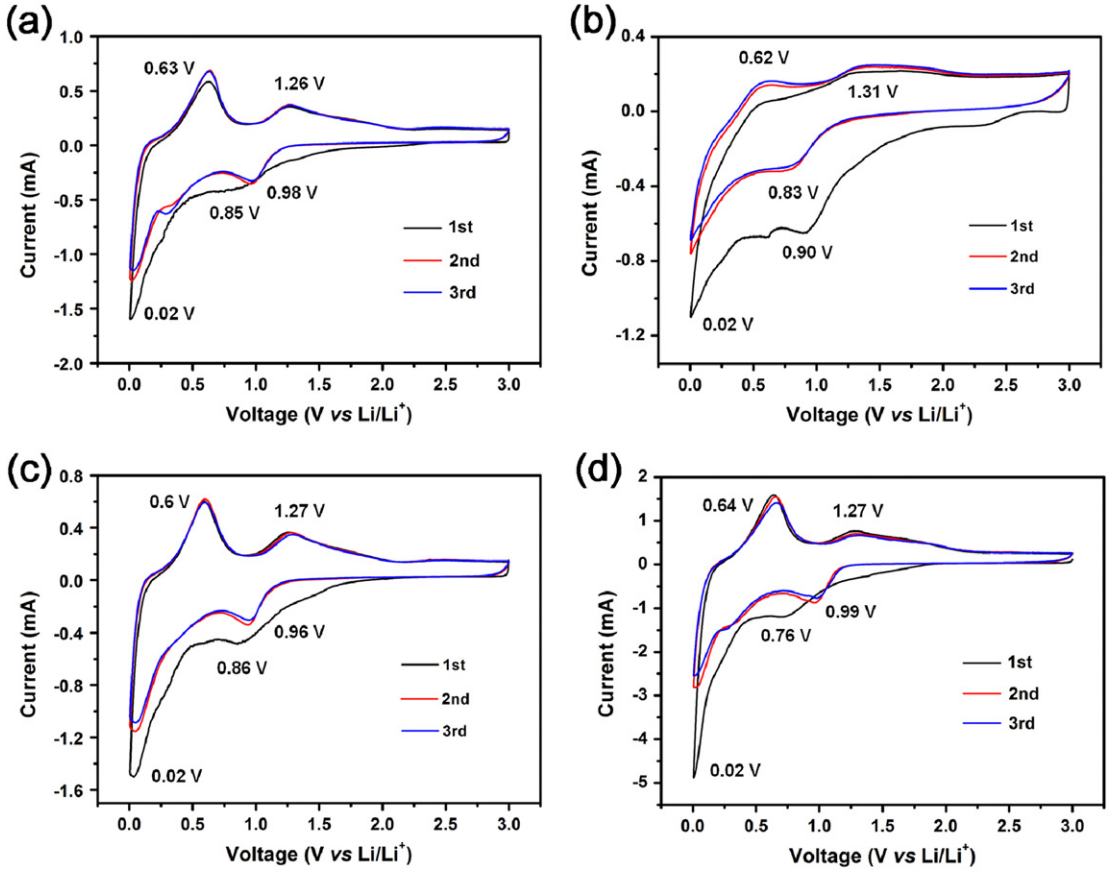

Figure 4. CV curves of the first three cycles of the SnO_2/G-3.3 (a), SAE SnO_2/G-1.7 (b), SAE SnO_2/G-3.3 (c) and SAE SnO_2/G-6.7 (d) electrodes at a scan rate of 0.5 mV s^{-1}.

After the first cycle, the CV curves of the composites are almost overlapped, implying the good reversibility of the electrochemical reactions on the electrodes.

Figure 5 shows the galvanostatic charge-discharge profiles of the SnO_2/G and SAE SnO_2/G electrodes at a current density of 100 mA g^{-1}. The capacity values were calculated based on the mass of the composite. Notably, the first discharge capacity for the SnO_2/G-3.3, SAE SnO_2/G-1.7, SAE SnO_2/G-3.3 and SAE SnO_2/G-6.7 electrodes is 1779, 1755, 2033 and 1821 mAh g^{-1}, corresponding to the coulombic efficiency of 62%, 47%, 56% and 59%, respectively. The initial irreversible capacity loss is attributed to the SEI formation and irreversible reactions on the electrodes. However, after the first cycle, the electrochemical reactions become more and more reversible upon cycling, leading to the significantly increased coulombic efficiency (figure S2). This is highly consistent with the CV results.

The cycling performance of SnO_2/G and SAE SnO_2/G electrodes was investigated at a current rate of 100 mA g^{-1}, as shown in figure 6(a). It can be seen that the SnO_2/G-3.3 electrode delivers a high initial reversible capacity of 1110 mAh g^{-1}. However, a rapid capacity fading is observed from the 30th cycles because of the severe pulverization of the electrode caused by the significant volume change during the charge and discharge process. The charge capacity of SnO_2/G-3.3 electrode is only 582 mAh g^{-1} after 120 cycles, which is 52.4% retention of the reversible capacity. The poor cycling stability of the SnO_2/G-3.3 electrode might be attributed to the inhomogeneous distribution of the SnO_2 nanoparticles on graphene sheets, as is observed by previous SEM and TEM images. Thus, the graphene matrix cannot effectively buffer the associated volume changes. In particular, the SAE SnO_2/G electrodes exhibit greatly improved cyclic stability over that of the SnO_2/G-3.3. It is worth noting that the electrochemical performances of SAE SnO_2/G correlate closely to the content of graphene in the composite. The SAE SnO_2/G-3.3 electrode with a graphene loading content of 24% displays the best Li storage performance in terms of high reversible capacity and good cycling stability. After 120 cycles, the SAE SnO_2/G-3.3 electrode can sustain a high reversible capacity of 998 mAh g^{-1}, 87.5% retention of the initial reversible capacity, which suggests its good cycling stability. The gradual increase of capacity from the 10th to 60th cycles could be attributed to the improved access of Li ions into the electrode, leading to an increased accommodation behavior for Li [41, 42]. Further increasing the graphene content in the composite (SAE SnO_2/G-1.7) will result in low Li storage

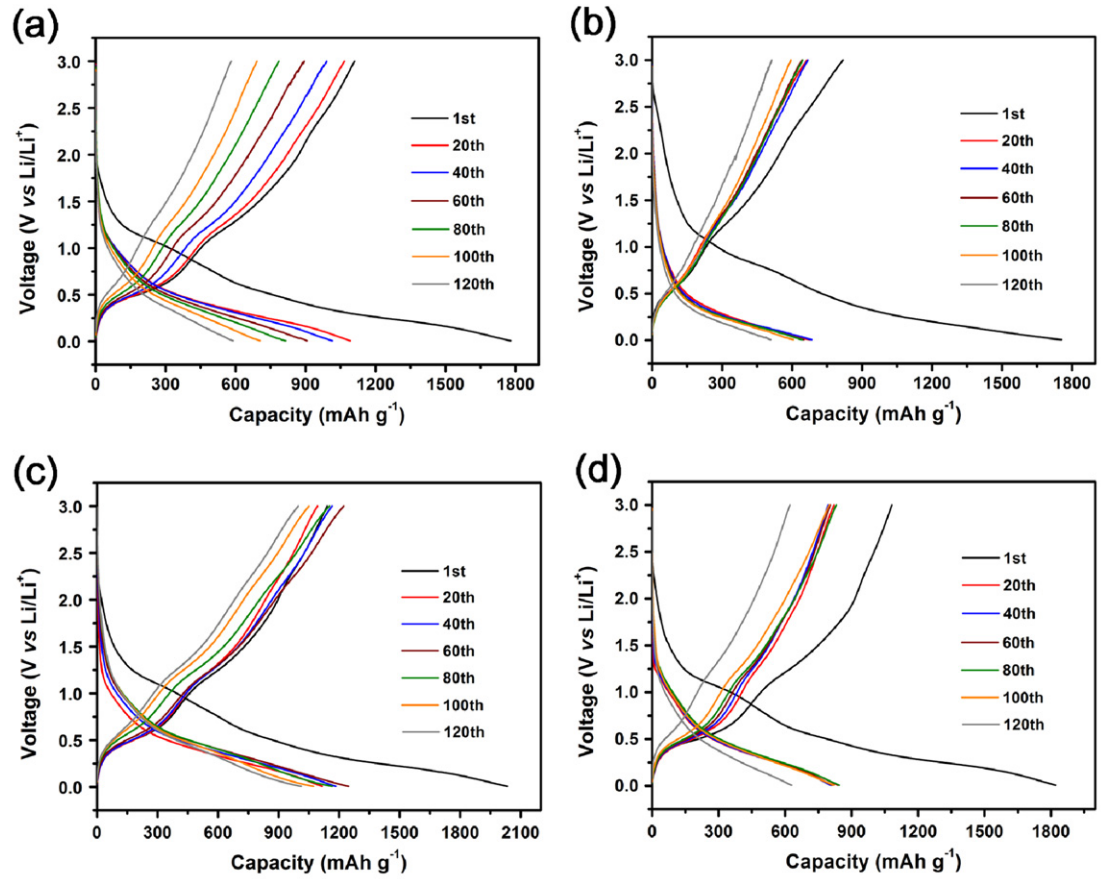

Figure 5. Galvanostatic charge-discharge profiles of SnO_2/G-3.3 (a), SAE SnO_2/G-1.7 (b), SAE SnO_2/G-3.3 (c) and SAE SnO_2/G-6.7 (d) electrodes at a current density of 100 mA g^{-1}.

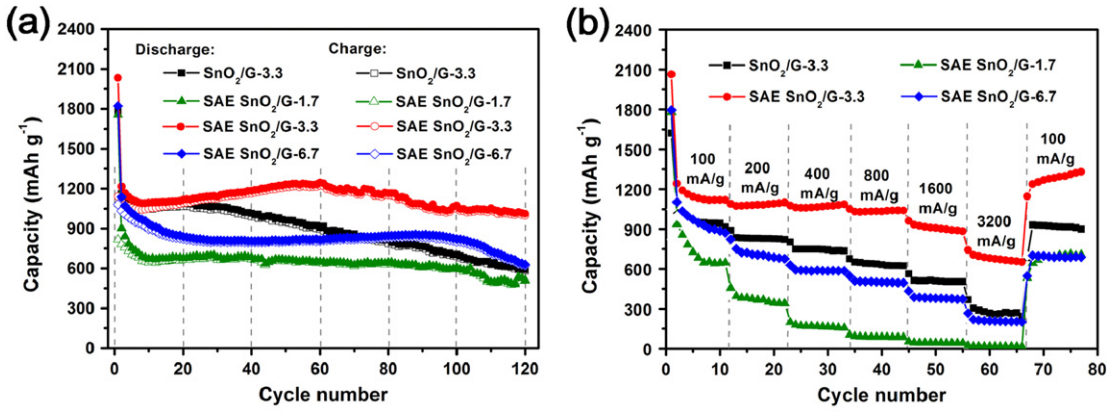

Figure 6. (a) Cycling performance of the SnO_2/G and SAE SnO_2/G electrodes at a current density of 100 mA g^{-1}. (b) Rate capability of the SnO_2/G and SAE SnO_2/G electrodes at various current densities.

capacity, while decreasing the graphene content (SAE SnO_2/G-6.7) will lead to poor cycling stability.

The rate capability of the SnO_2/G and SAE SnO_2/G electrodes was evaluated at stepwise current densities (figure 6(b)). As the current densities increase from 100 to 200, 400, 800, 1600 and 3200 mA g^{-1}, the SAE SnO_2/G-3.3 electrode still exhibits stable capacities of 1144, 1078, 1073, 1032, 910 and 682 mAh g^{-1}, respectively. Moreover, with the current density returns to 100 mA g^{-1}, the capacity of the electrode is able to recover to its initial value, indicating its excellent rate capability. As far as we know, such superior Li storage performance is rarely reported in the SnO_2/G composites, as summarized in table S1. Remarkably, the SAE SnO_2/G-3.3 electrode always delivers higher capacities than the other electrodes at various current densities (also shown in figure S3). EIS measurements (figure 7) illustrate that the charge transfer resistance of SAE

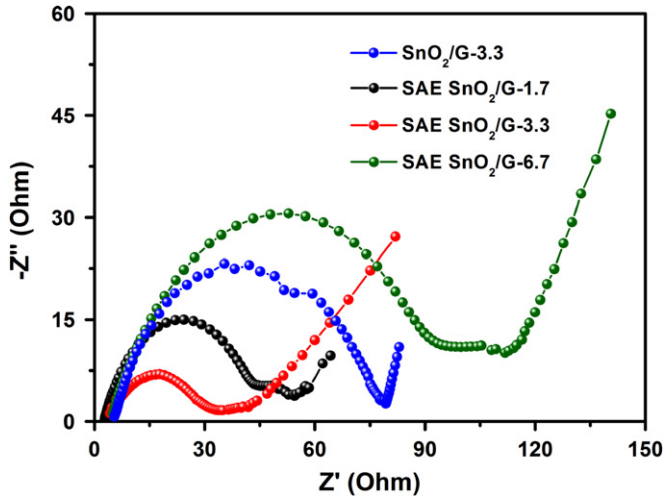

Figure 7. Nyquist plots of the SnO_2/G and SAE SnO_2/G electrodes.

SnO_2/G-3.3 electrode is 37 Ω, which is much smaller than the SnO_2/G-3.3 (79 Ω), SAE SnO_2/G-1.7 (54 Ω) and SAE SnO_2/G-6.7 (111 Ω) electrodes.

The excellent electrochemical performances of the SAE SnO_2/G-3.3 composite can be attributed to its unique structural features. First of all, the intrinsic activity of the SnO_2 nanoparticles component in the composite endows high Li storage capacity by providing large interfacial areas for fast Li insertion/extraction within the electrode, and shortening the solid-state diffusion length of Li ions. In addition, the uniform distribution of SnO_2 nanoparticles on graphene sheets can effectively prevent the agglomeration Sn particles formed during Li insertion. Secondly, the graphene component in the composite can act as not only continuous channels for electrons transport but also Li storage material, which additionally contributes to its exceptional performance. More importantly, the random aggregation of graphene sheets results in the encapsulation of SnO_2 nanoparticles in graphene layers, producing a mechanically robust structure. Therefore, the graphene sheets can function as a 3D scaffold for preventing the SnO_2 nanoparticles being peeled off and buffering the associated volume changes.

4. Conclusions

In summary, we have developed a facile and effective approach to synthesize SnO_2/G composite through a surfactant-assisted redox method. This composite is composed of uniform SnO_2 nanoparticles with a size of ~5 nm, which are homogeneously encapsulated in the graphene layers. Benefiting from the unique structural features, the composite exhibits high reversible capacity (1141 mAh g^{-1} at a current density of 100 mA g^{-1}) and long-term cycling stability (120 cycles with 87.5% retention), as well as excellent rate capability when applied as the anode material for LIBs. Considering the simple, low cost and high throughput fabrication process of this approach, we believe the composite may be a promising alternative anode material for next generation high-performance LIBs. Moreover, our strategy could also be helpful in fabricating other graphene-based composites for diverse applications.

Acknowledgments

This work is supported by the Singapore National Research Foundation under NRF RF Award No. NRFRF2010-07, A*Star SERC PSF grant 1321202101 and MOE Tier 2 MOE2012-T2-2-049. WH gives thanks for the support by the Natural Science Foundation of Jiangsu Province (BM2012010), Priority Academic Program Development of Jiangsu Higher Education Institutions (YX03001), Ministry of Education of China (IRT1148), Synergetic Innovation Center for Organic Electronics and Information Displays, and the National Natural Science Foundation of China (61136003, 51173081).

References

[1] Van Noorden R 2014 A better battery *Nature* **507** 26–8
[2] Ai W, Luo Z, Jiang J, Zhu J, Du Z, Fan Z, Xie L, Zhang H, Huang W and Yu T 2014 Nitrogen and sulfur codoped graphene: multifunctional electrode materials for high-performance Li-ion batteries and oxygen reduction reaction *Adv. Mater.* **26** 6186–92
[3] Wang H and Rogach A L 2013 Hierarchical SnO_2 nanostructures: recent advances in design, synthesis, and applications *Chem. Mater.* **26** 123–33
[4] Huang J Y *et al* 2010 In situ observation of the electrochemical lithiation of a single SnO_2 nanowire electrode *Science* **330** 1515–20
[5] Arico A S, Bruce P, Scrosati B, Tarascon J M and van Schalkwijk W 2005 Nanostructured materials for

advanced energy conversion and storage devices *Nat. Mater.* **4** 366–77
[6] Yu C, Yu J C, Wang F, Wen H and Tang Y 2010 Growth of single-crystalline SnO_2 nanocubes via a hydrothermal route *CrystEngComm.* **12** 341–3
[7] Wang J, Du N, Zhang H, Yu J and Yang D 2011 Large-scale synthesis of SnO_2 nanotube arrays as high-performance anode materials of Li-ion batteries *J. Phys. Chem.* C **115** 11302–5
[8] Park M S, Wang G X, Kang Y M, Wexler D, Dou S X and Liu H K 2007 Preparation and electrochemical properties of SnO_2 nanowires for application in lithium-ion batteries *Angew. Chem. Int. Ed.* **46** 750–3
[9] Yu Y, Gu L, Dhanabalan A, Chen C H and Wang C 2009 Three-dimensional porous amorphous SnO_2 thin films as anodes for Li-ion batteries *Electrochim. Acta* **54** 7227–30
[10] Lou X W, Wang Y, Yuan C, Lee J Y and Archer L A 2006 Template-free synthesis of SnO_2 hollow nanostructures with high lithium storage capacity *Adv. Mater.* **18** 2325–9
[11] Zhou W, Tay Y Y, Jia X, Yau Wai D Y, Jiang J, Hoon H H and Yu T 2012 Controlled growth of SnO_2@Fe_2O_3 double-sided nanocombs as anodes for lithium-ion batteries *Nanoscale* **4** 4459–63
[12] Chen Y, Lu J, Shi W, Lu L and Xue J 2014 Synthesis of SnO_2/MoS_2 composites with different component ratios and their applications as lithium ion battery anodes *J. Mater. Chem.* A **2** 17857–66
[13] Wang X *et al* 2012 N-doped graphene-SnO_2 sandwich paper for high-performance lithium-ion batteries *Adv. Funct. Mater.* **22** 2682–90
[14] Zhu J, Jiang J, Feng Y, Meng G, Ding H and Huang X 2013 Three-dimensional Ni/SnOx/C hybrid nanostructured arrays for lithium-ion microbattery anodes with enhanced areal capacity *ACS Appl. Mater. Inter.* **5** 2634–40
[15] Liu X, Wu M, Li M, Pan X, Chen J and Bao X 2013 Facile encapsulation of nanosized SnO_2 particles in carbon nanotubes as an efficient anode of Li-ion batteries *J. Mater. Chem.* A **1** 9527–35
[16] Chen B, Qian H, Xu J, Qin L, Wu Q H, Zheng M and Dong Q 2014 Study on SnO_2/graphene composites with superior electrochemical performance for lithium-ion batteries *J. Mater. Chem.* A **2** 9345–52
[17] Bai H, Li C and Shi G 2011 Functional composite materials based on chemically converted graphene *Adv. Mater.* **23** 1089–115
[18] Ai W, Xie L, Du Z, Zeng Z, Liu J, Zhang H, Huang Y, Huang W and Yu T 2013 A novel graphene-polysulfide anode material for high-performance lithium-ion batteries *Sci. Rep.* **3** 2341
[19] Lee B, Han S C, Oh M, Lah M S, Sohn K S and Pyo M 2013 Tin dioxide nanoparticles impregnated in graphite oxide for improved lithium storage and cyclability in secondary ion batteries *Electrochim. Acta* **113** 149–55
[20] Cai D, Yang T, Liu B, Wang D, Liu Y, Wang L, Li Q and Wang T 2014 A nanocomposite of tin dioxide octahedral nanocrystals exposed to high-energy facets anchored onto graphene sheets for high performance lithium-ion batteries *J. Mater. Chem.* A **2** 13990–5
[21] Paek S M, Yoo E and Honma I 2008 Enhanced cyclic performance and lithium storage capacity of SnO_2/graphene nanoporous electrodes with three-dimensionally delaminated flexible structure *Nano Lett.* **9** 72–5
[22] Zhao B, Zhang G, Song J, Jiang Y, Zhuang H, Liu P and Fang T 2011 Bivalent tin ion assisted reduction for preparing graphene/SnO_2 composite with good cyclic performance and lithium storage capacity *Electrochim. Acta* **56** 7340–6
[23] Wang X, Zhou X, Yao K, Zhang J and Liu Z 2011 A SnO_2/graphene composite as a high stability electrode for lithium ion batteries *Carbon* **49** 133–9
[24] Chen Z, Zhou M, Cao Y, Ai X, Yang H and Liu J 2012 In situ generation of few-layer graphene coatings on SnO_2-SiC core–shell nanoparticles for high-performance lithium-ion storage *Adv. Energy Mater.* **2** 95–102
[25] Zhang C, Peng X, Guo Z, Cai C, Chen Z, Wexler D, Li S and Liu H 2012 Carbon-coated SnO_2/graphene nanosheets as highly reversible anode materials for lithium ion batteries *Carbon* **50** 1897–903
[26] Patil S, Patil V, Sathaye S and Patil K 2014 Facile room temperature methods for growing ultra thin films of graphene nanosheets, nanoparticulate tin oxide and preliminary assessment of graphene-tin oxide stacked layered composite structure for supercapacitor application *RSC Adv.* **4** 4094–104
[27] Vinayan B P and Ramaprabhu S 2013 Facile synthesis of SnO_2 nanoparticles dispersed nitrogen doped graphene anode material for ultrahigh capacity lithium ion battery applications *J. Mater. Chem.* A **1** 3865–71
[28] Zhou X, Wan L J and Guo Y G 2013 Binding SnO_2 nanocrystals in nitrogen-doped graphene sheets as anode materials for lithium-ion batteries *Adv. Mater.* **25** 2152–7
[29] Ai W, Zhou W, Du Z, Du Y, Zhang H, Jia X, Xie L, Yi M, Yu T and Huang W 2012 Benzoxazole and benzimidazole heterocycle-grafted graphene for high-performance supercapacitor electrodes *J. Mater. Chem.* **22** 23439–46
[30] Li F H, Song J F, Yang H F, Gan S Y, Zhang Q X, Han D X, Ivaska A and Niu L 2009 One-step synthesis of graphene/SnO_2 nanocomposites and its application in electrochemical supercapacitors *Nanotechnology* **20** 455602
[31] Li Y, Lv X, Lu J and Li J 2010 Preparation of SnO_2-nanocrystal/graphene-nanosheets composites and their lithium storage ability *J. Phys. Chem.* C **114** 21770–4
[32] Ahn H J, Choi H C, Park K W, Kim S B and Sung Y E 2004 Investigation of the structural and electrochemical properties of size-controlled SnO_2 nanoparticles *J. Phys. Chem.* B **108** 9815–20
[33] Humaira S, Kemp K C, Vimlesh C and Kwang S K 2012 Graphene-SnO_2 composites for highly efficient photocatalytic degradation of methylene blue under sunlight *Nanotechnology* **23** 355705
[34] Smith R D L, Prevot M S, Fagan R D, Zhang Z, Sedach P A, Siu M K J, Trudel S and Berlinguette C P 2013 Photochemical route for accessing amorphous metal oxide materials for water oxidation catalysis *Science* **340** 60–3
[35] Ai W *et al* 2014 Redox-crosslinked graphene networks with enhanced electrochemical capacitance *J. Mater. Chem.* A **2** 12924–30
[36] Sun L, Tian C, Li M, Meng X, Wang L, Wang R, Yin J and Fu H 2013 From coconut shell to porous graphene-like nanosheets for high-power supercapacitors *J. Mater. Chem.* A **1** 6462–70
[37] Zheng X, Lv W, He Y B, Zhang C, Wei W, Tao Y, Li B and Yang Q H 2014 3D hollow Sn@carbon-graphene hybrid material as promising anode for lithium-ion batteries *J. Nanomater.* **2014** 974285
[38] Hong Y J, Son M Y and Kang Y C 2013 One-pot facile synthesis of double-shelled SnO_2 yolk-shell-structured powders by continuous process as anode materials for Li-ion batteries *Adv. Mater.* **25** 2279–83
[39] Sandu I, Brousse T, Schleich D M and Danot M 2006 The chemical changes occurring upon cycling of a SnO_2 negative electrode for lithium ion cell: in situ mossbauer investigation *J. Solid State Chem.* **179** 476–85
[40] Di Lupo F, Gerbaldi C, Meligrana G, Bodoardo S and Penazzi N 2011 Novel SnO_2/mesoporous carbon spheres composite anode for Li-ion batteries *Int. J. Electrochem. Sci.* **6** 3580–93
[41] Du Z, Ai W, Xie L and Huang W 2014 Organic radical functionalized graphene as a superior anode material for lithium-ion batteries *J. Mater. Chem.* A **2** 9164–8
[42] Ai W, Du Z, Fan Z, Jiang J, Wang Y, Zhang H, Xie L, Huang W and Yu T 2014 Chemically engineered graphene oxide as high performance cathode materials for Li-ion batteries *Carbon* **76** 148–54